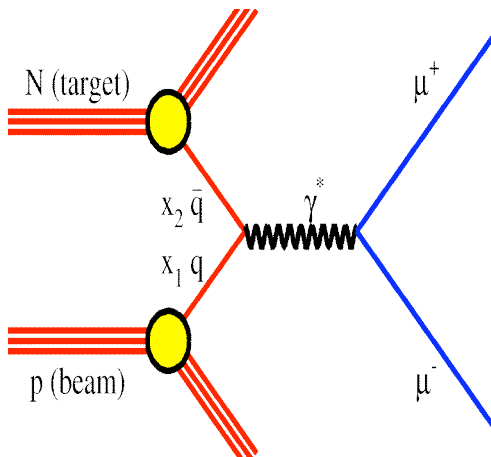


## Fermilab E906: Hodoscopes for Stations 3 and 4

**Donald Isenhower**

**Abilene Christian University**

**Abilene, Texas U.S.A.**

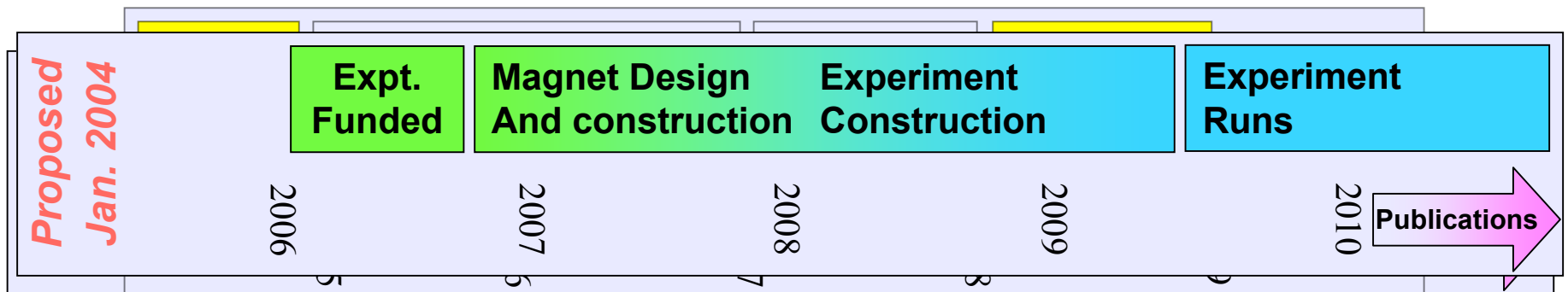


- *Use in trigger*
- *Construction*
- *Electronics readout via FPGA*
- *Attempt at 100% livetime trigger*
- *Relationship between E906 and SBIR Phase II*

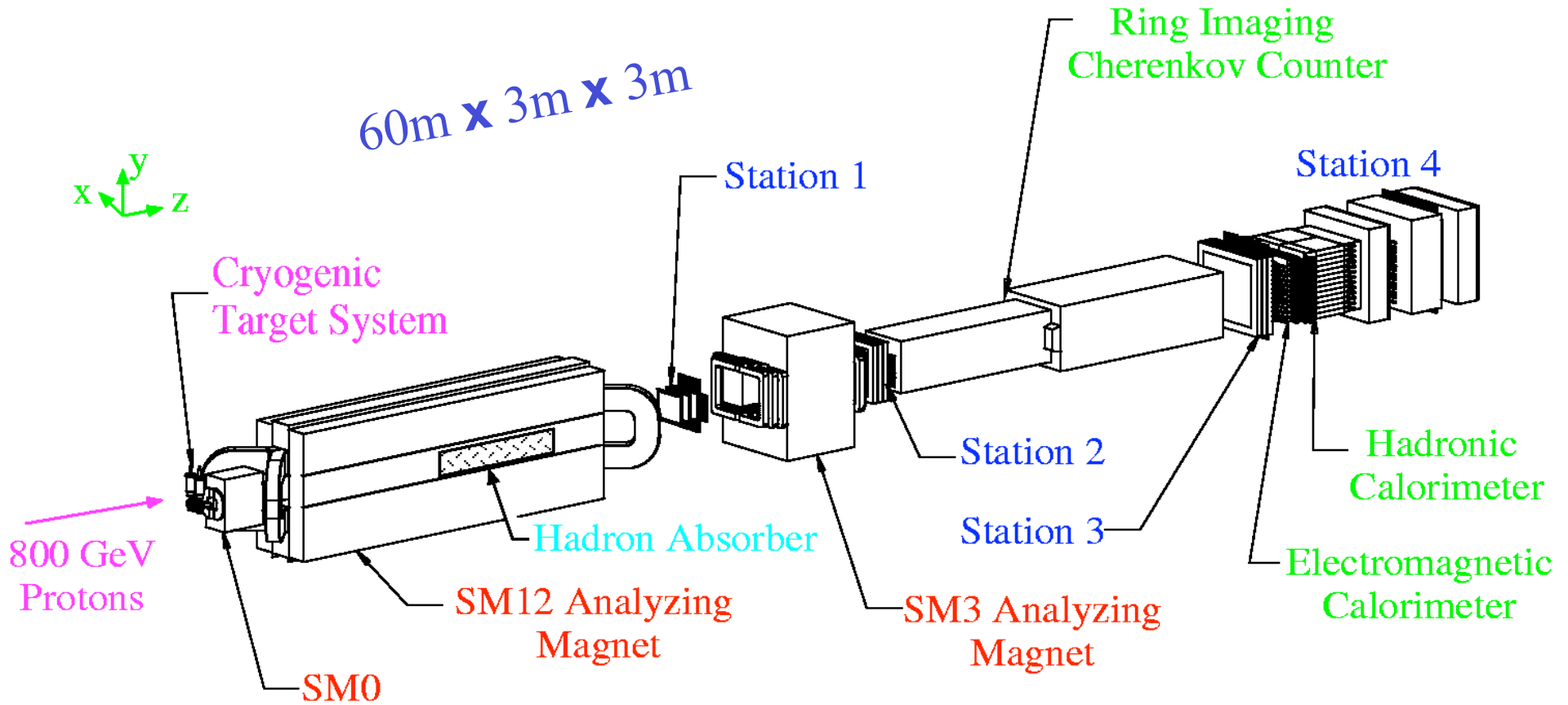
Slides are a compilation of many different talks at different places.

Special thanks to Paul Reimer.

# *E906 Scheduling Plans in the Past*



## Comparison of the two detectors: Fermilab E866/NuSea Detector



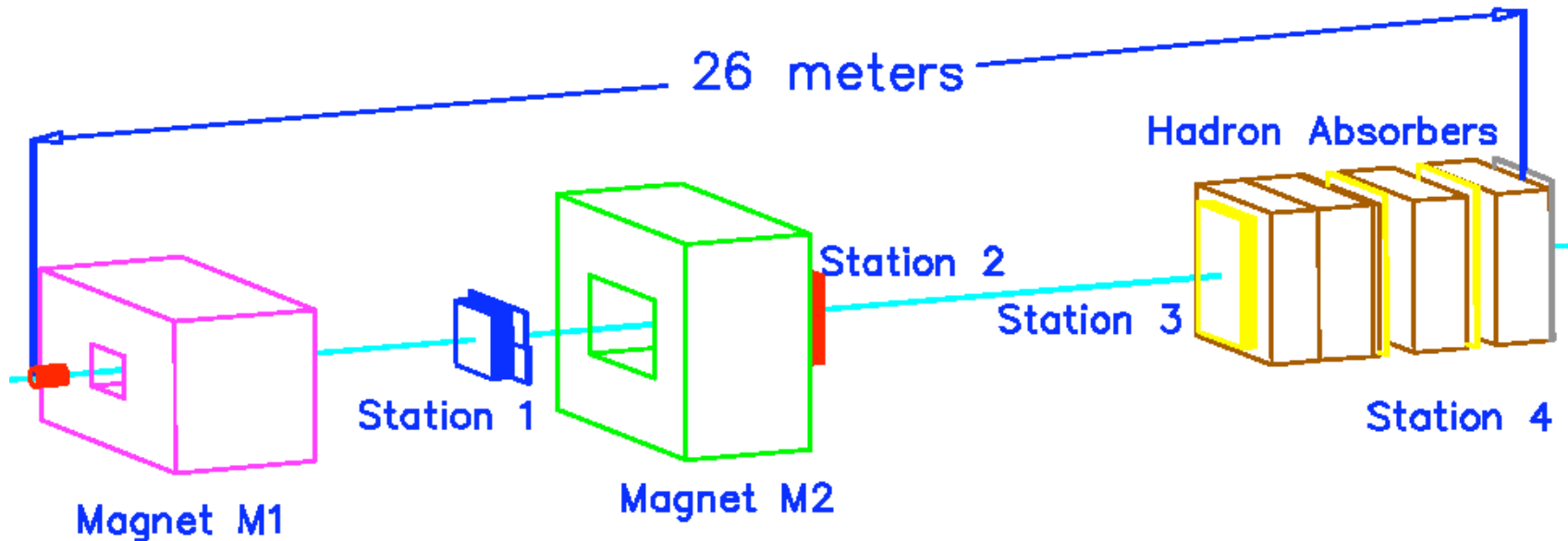
- Forward  $x_F$ , high mass  $\mu$ -pair spectrometer
- Liquid hydrogen and deuterium targets
- Two acceptance defining magnets (SM0, SM12)
- Also used solid W, Be, Fe targets

- Beam dump (4.3m Cu)
- Hadronic absorber (13.4  $I_0$ -Cu, C, CH<sub>2</sub>)
- Momentum analyzing magnet (SM3)
- Three tracking stations
- Muon identifier wall & 4<sup>th</sup> tracking

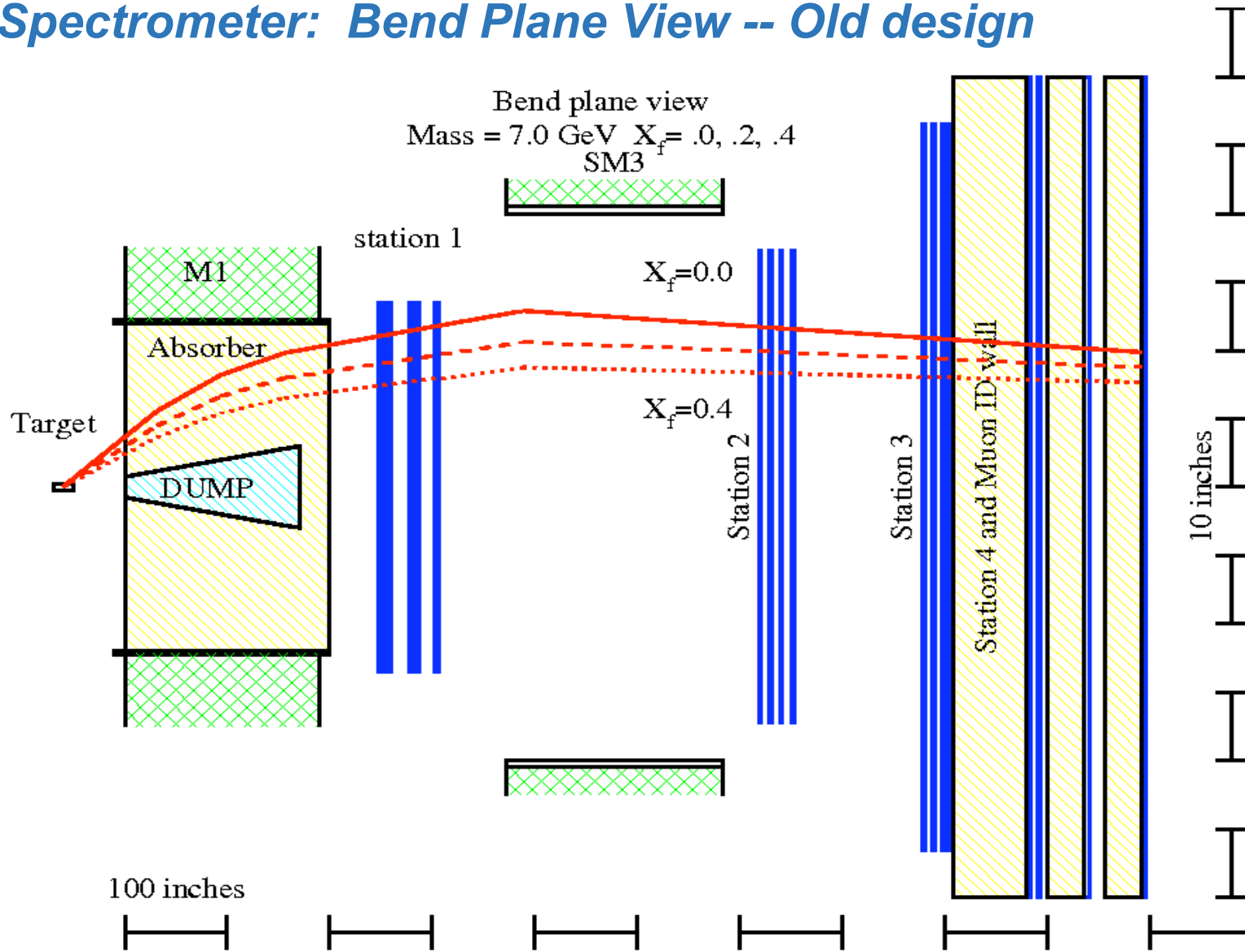
## E906 Apparatus (old open design)

Replacement of old hodoscopes:

1. Stations 1 & 2 scintillator are being replaced because they are the wrong size and are too thin to produce enough light to deal with fringe fields of M1 and M2.
2. Stations 3 & 4 scintillators are being replaced because they are the wrong size and are old enough that they will craze very badly if any work is done on them.
3. There are also changes being made in order to improve the trigger.



# E906 Spectrometer: Bend Plane View -- Old design





## *Comments on changes needed for detector sizes compared to original proposal for better statistics*

- Proposal contains tables of planned sizes of each detector.
- Sizes change if z-position is changed (this is obvious).
- But looking closer one finds something we missed. In the summer of 2007, Nathan Sparks (ACU), working with Paul Reimer and Chuck Brown, found out that ignoring events where a muon went through the coils was costing us acceptance.
- Next slide shows effects of slight increases in detector size. It does not evaluate separately each detector component. It just scales every detector up in size by a specific fraction.

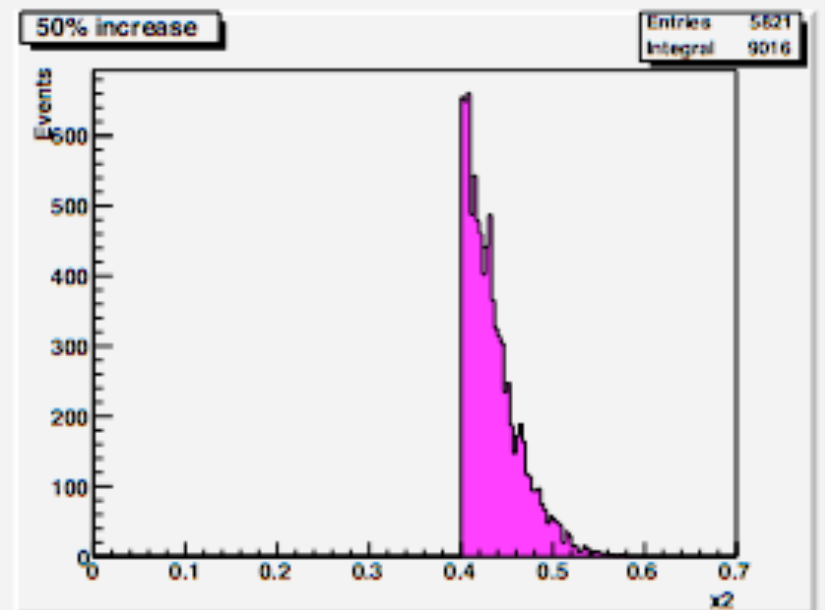
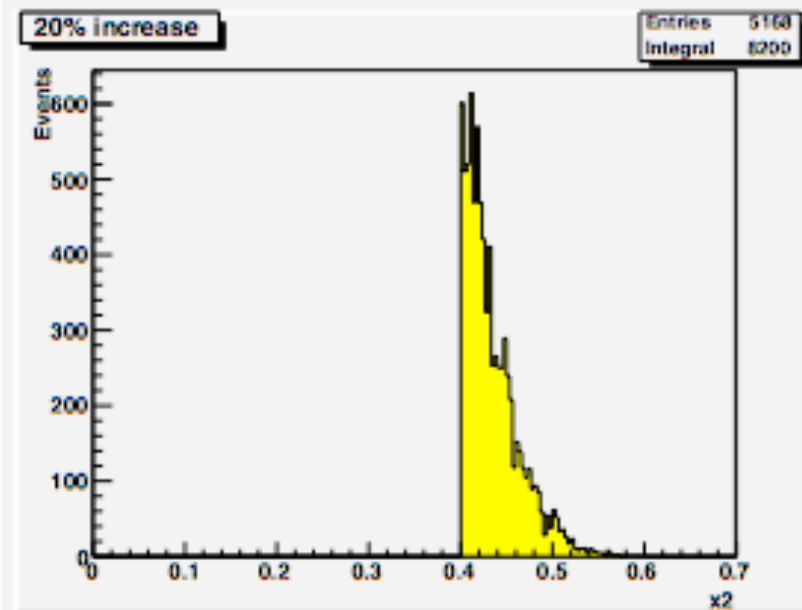
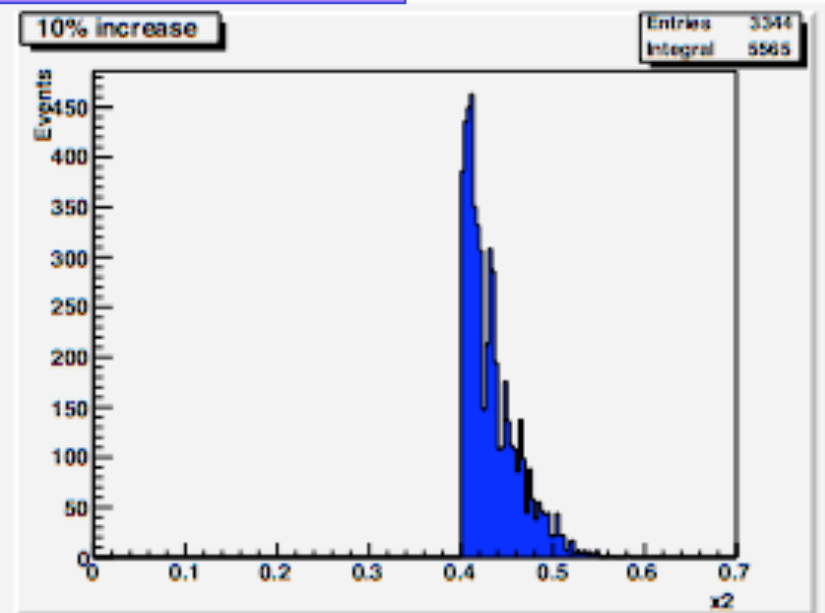
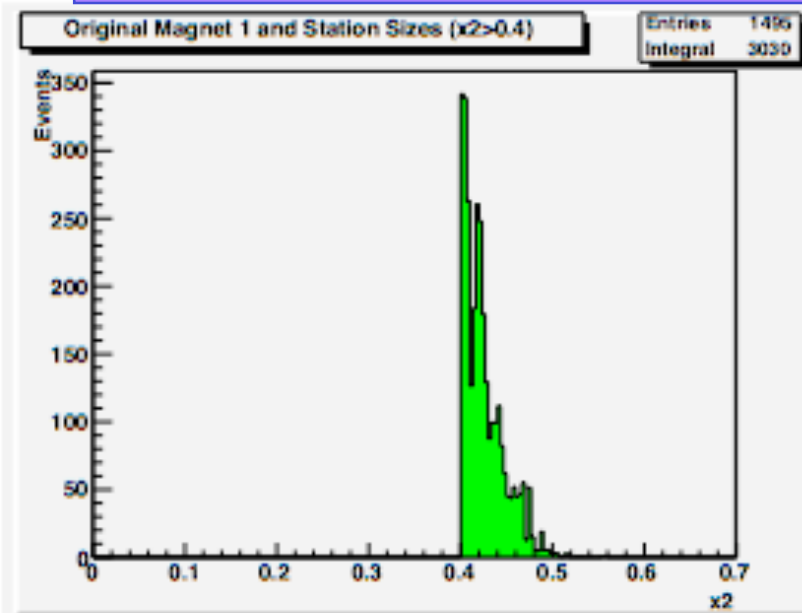


# Fine tuning of acceptance, tracking through M1 coils

1,495 events pass through "normal" acceptance for  $x_2 > 0.4$

Add 10% --> 3,344 evts; Add 20% --> 5,168 evts; Add 50% --> 5,821 evts.

Work done by  
Nathan Sparks  
(ACU), summer  
2007.



Collaboration

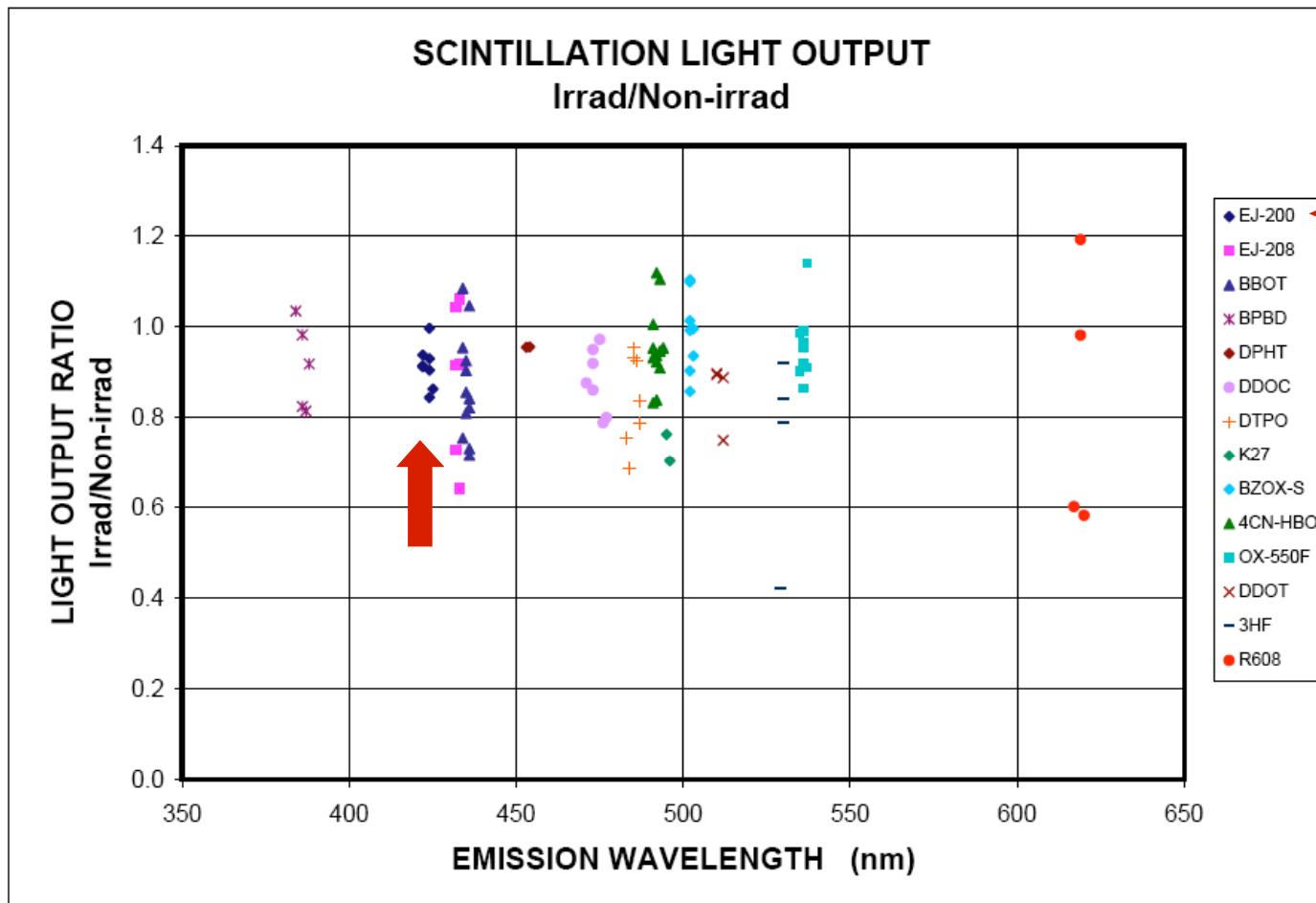
## *Some details on Stations 3 and 4*

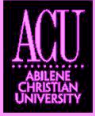
- Each plane will have 2x16 scintillators (split up/down or left/right).
- Every paddle will be double ended (this is dictated by the trigger).
- Each will be read out via an FPGA based TPC (design will borrow heavily from Pat McGaughey's design for station 4 DCs).
- TDCs will be multihit with 0.25ns resolution (easily done with even a low end FPGA (with a 100 MHz FPGA one can get approximately 0.04ns).
- See proposal for details on how these were planned for the trigger.
- Will be made from Eljen scintillator, each piece will be diamond milled (Eljen Corp. is about 60 km from Abilene, so they will be convenient for us).

# Details on EJ-200 Scintillator

(note: Charles Hurlbut at Eljen is the one who founded Bicron's plastic scintillator division and developed many of their scintillator materials)

## ELJEN TECHNOLOGY





## *Comments on ACU FPGA Programming Project*

- The U.S. government funds Small Business Innovative Research (SBIR) projects. Every funding agency must set aside ~1.5% of their budget for these projects.
- DOE Nuclear Physics is of course one of these agencies.
- Donald Isenhower and Shon Watson (ACU technician) are working with a new company called Innovation Partners and have just completed a Phase I (\$100k) grant showing the feasibility of a method to decrease the time to produce FPGA code.
- A Phase II proposal (\$750k) has been submitted to apply what was learned in Phase I to make viable product. It is planned to use E906 as the main nuclear physics experiment to produce a prototype that would perform as the readout for the hodoscope planes.
- Hardware design will be based on work done by Pat McGaughey for the E906 drift chambers and the PHENIX Forward Vertex detector.

## What is the problem?

### 3.2 The FPGA Design Problem

The problem, however, is that the traditional FPGA design flow is not well suited to scientists. Scientists are gifted individuals who have great depth in their domain of expertise and utilize custom software in their experiments. Unfortunately, the traditional FPGA design flow does not capitalize on this capability and requires that a *hardware description language* (e.g. VHDL and Verilog) be used to design the FPGA. VHDL and Verilog are not just another syntax for creating sequential programs but are low-level circuit description languages that require the designer to have a detailed understanding of parallel logic design. Additionally, these languages are technology dependent and have to be rewritten for each new FPGA device. For example, the code for a 100MHz FPGA does not work well for a newer 200 MHz FPGA as the technology changes and new hardware resources, such as multiply-accumulate blocks, are available to the designer. To achieve peak FPGA processing rates, as is needed by DAQ systems, the designers must exploit all of the available resources in the FPGA.

FPGA designs are complex and are labor intensive. In 2005, EE Times performed a study of the design duration and costs associated with creating FPGA designs. As shown in Figure 2, only 9% of the designs were completed in 3 months, 17% in 3 to 6 months, and 47% required 6 to 12 months. 27% required more than a year to complete. The median design time was 9 months.

Figure 2 is not shown

## Examples of FPGA coding method

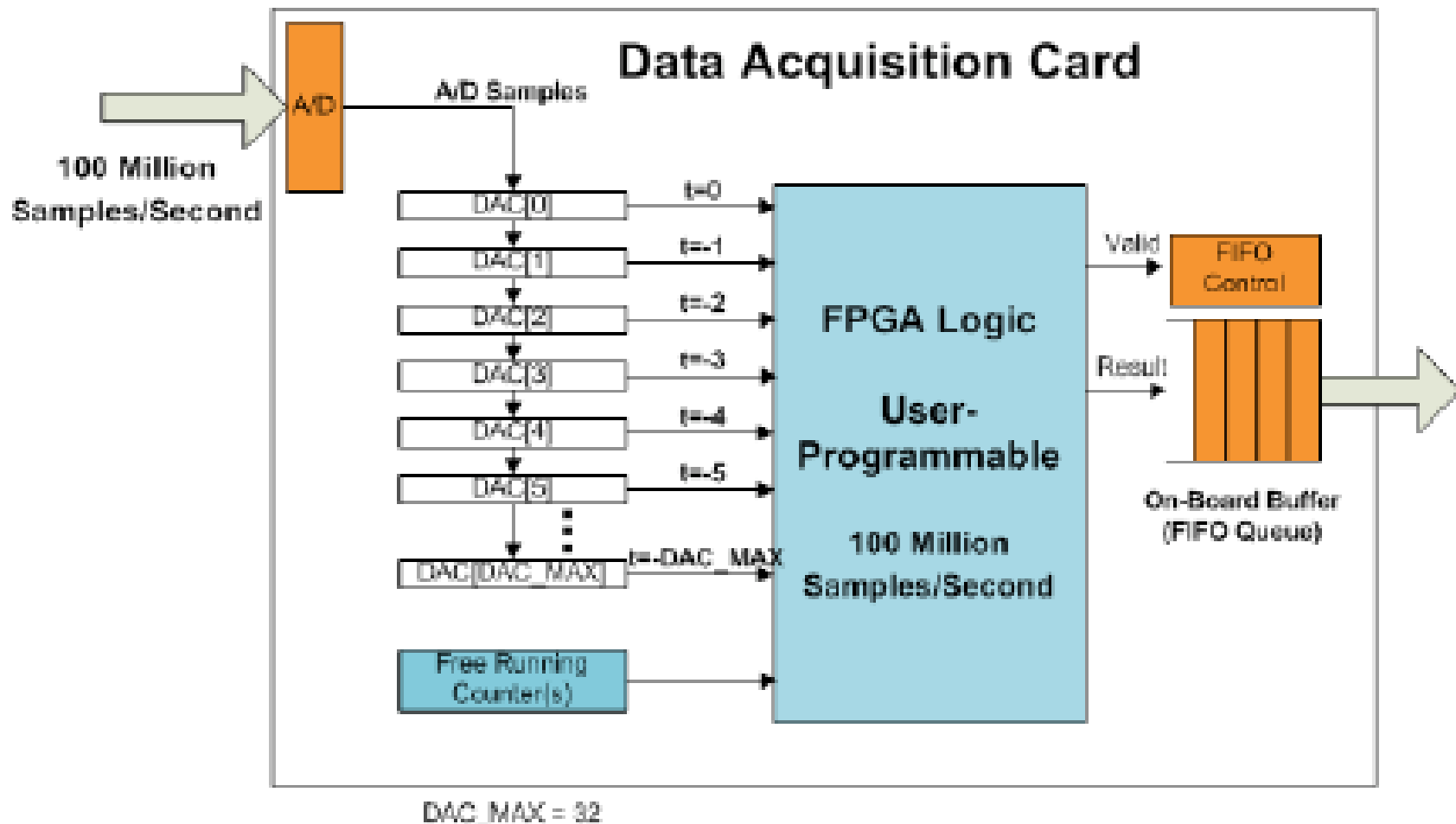


Figure 3: Concurrent EDA's DAQ Accelerator Hardware Framework. This diagram shows how samples from the A/D are fed into the User Programmable FPGA Logic. The out of the User Logic is fed into a FIFO that interfaces with the DAQ Hardware.

# Constant Fraction Discriminator

The examples below were done using a set of ADC samples.  
Both discriminator functions were done via software in an FPGA.  
 The CFD is a digital version of the analog circuit for a CFD.

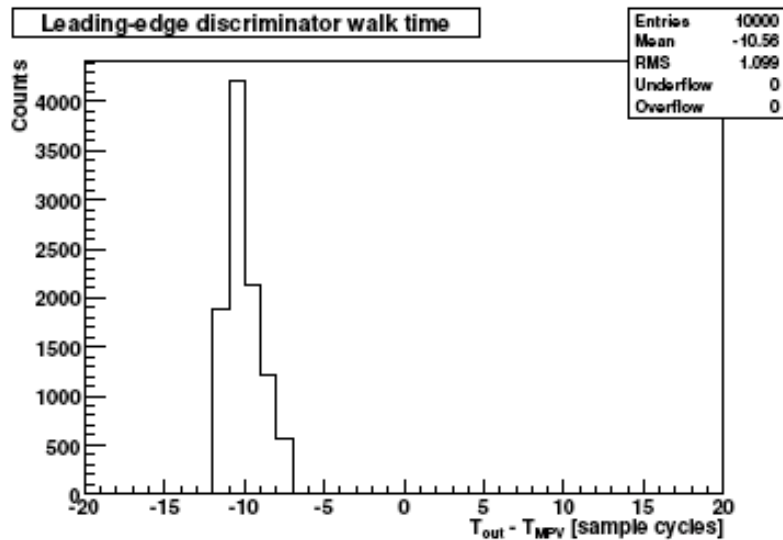


Figure 10: Systematically reduced timing resolution from a leading edge discriminator.

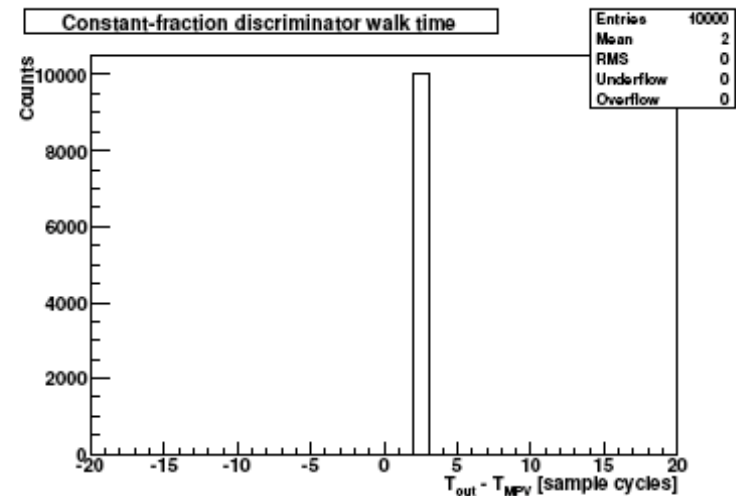


Figure 11: Single ADC clock-cycle precision timing resolution from a constant fraction discriminator.

# *Principal Component Analysis What is it?*

## 3.5 Principal component analysis

Component analysis techniques are generally used to reduce high-dimensional data to lower-dimensional representations. Principal component analysis (PCA) is a linear method to accomplish this task. In a physical system, PCA can often be used to extract dimensions that are most significant physically (i.e. separating interesting signals from noise or combining redundant measurements).

During Phase I, an example PCA was developed based on candidate tracks in a simplified version of the Fermilab E906 di-muon spectrometer. Geant4 was used to simulate particle tracks through the detector system. Figure 16 shows the detector geometry and simulated tracks. The basic premise of this example is the common generic PCA process might be used as a pre-processing filter in part of an advanced FPGA accelerated trigger system.

## Application to E906 ---> SeaQuest!

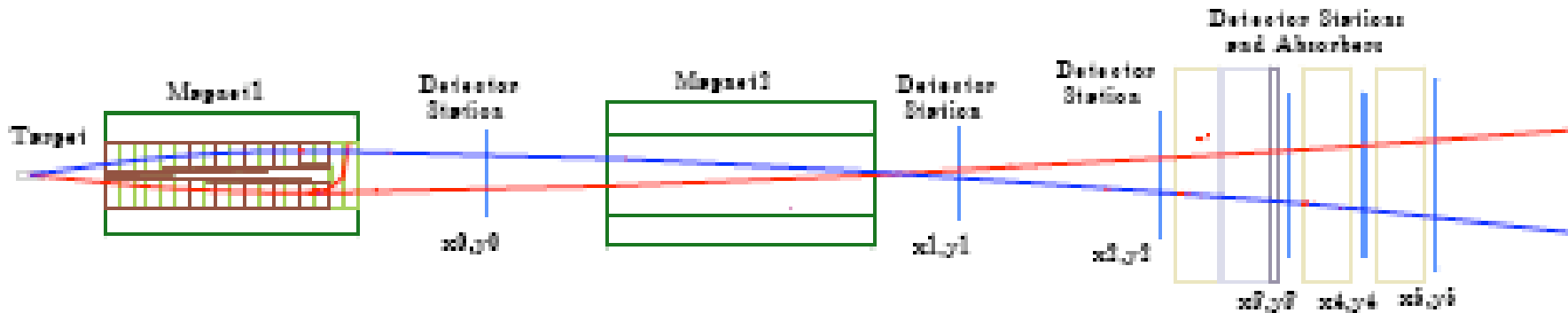


Figure 16: Simplified E906 di-muon spectrometer geometry from Geant4 simulation. The positive muon track is colored blue. Negative particle tracks (negative muon and ionization electrons) are colored red. For simplicity, this simulation assumes  $x$ - $y$  coordinates will be recorded at all six detector planes, while the actual experiment has some  $y$ -only planes. The length of the apparatus is approximately 26 meters.

## Principal Component Analysis Example

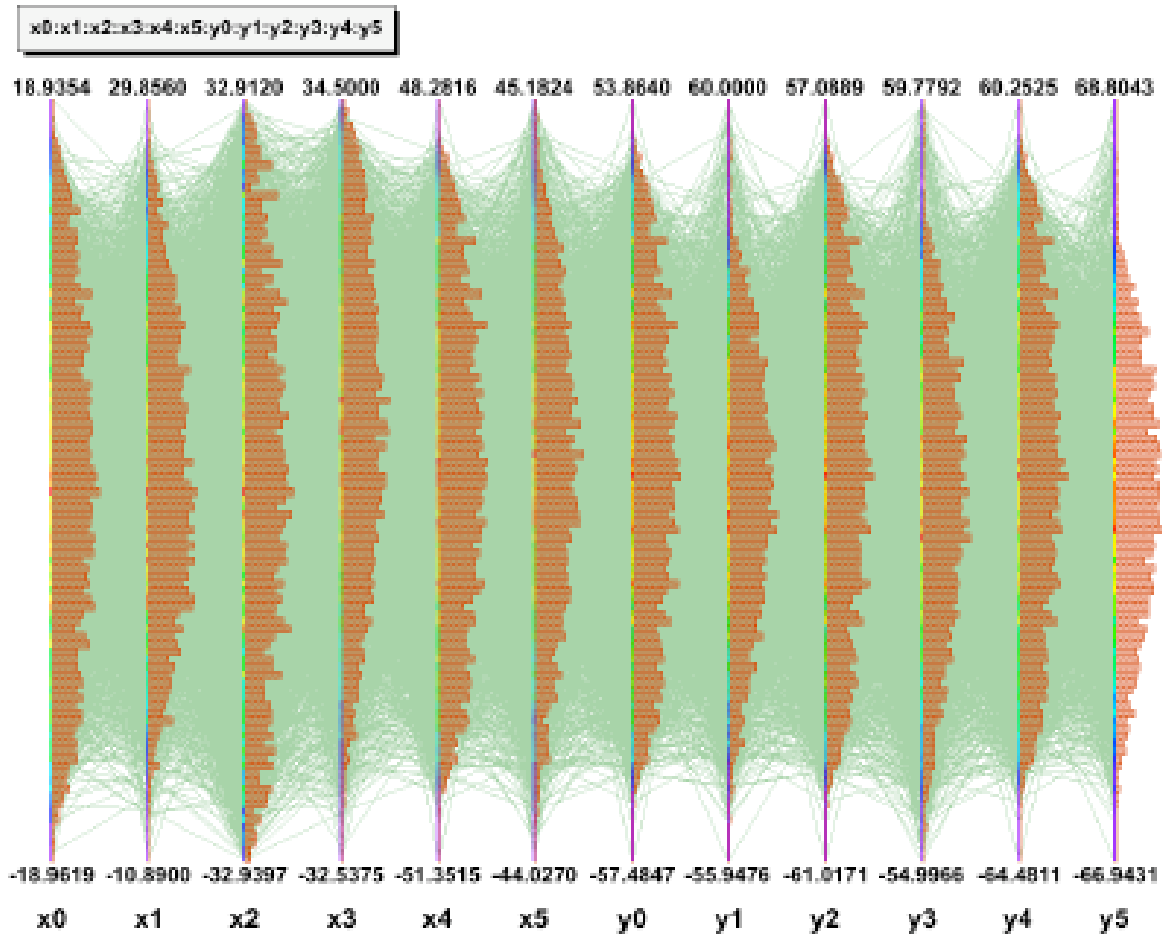


Figure 17: Parallel coordinate diagram showing the distribution of input  $x$  and  $y$  coordinates in the laboratory coordinate system for valid positive muon tracks. These values are measured in inches at each detector plane.

*Note that this operation takes 93 clock cycles, but once started, you get a new result on every clock cycle. So each new PCA result would be produced in 2ns with a 500MHz FPGA*

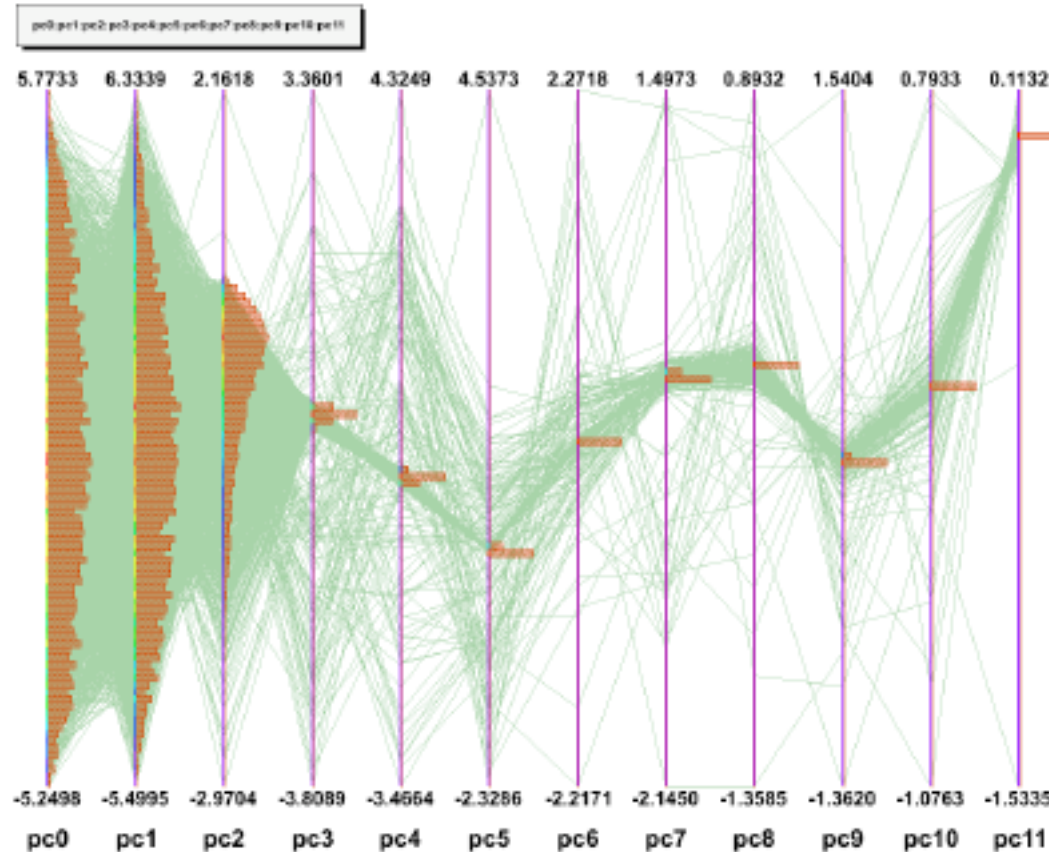
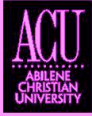


Figure 18: Parallel coordinate diagram showing the distribution of valid positive muon tracks that have been transformed into the principal coordinate space. The high order coordinates (pc9, pc10, pc11) are almost negligible for most valid tracks as most physical information is in the lowest three coordinates (pc0, pc1, pc2).

## *Why do we care about all this?*

- Almost every readout chain in E906 will be involve FPGAs.
- FPGAs work as a pipeline for data, so in principle it should be possible to design a trigger with zero deadtime.
- First level would come from hodoscopes.
- Second level would come from other detectors.
- Rutger's presentation shows how things have changed and are being made simpler by new FPGA designs. In many cases an FPGA demo board is adequate for a DAQ system.
- FPGAs are doubling in processing speed every year. LANL TDC boards have large number of channels at a very low cost. If SBIR Phase II is funded, we should be able to provide enough of these modules to read out all of the hodoscopes and be able to pass the information on to the Rutger's trigger module.
- Communication between modules is fast. Many FPGA's now come with dual 2.5Gbit ethernet connections.



## *Rates from old design*

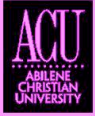
### *Solid Fe magnet shouldn't be too different*

	<i>LH<sub>2</sub></i> Target		<i>LD2</i> Target		Copper Beam Dump	
	$\mu$ 's	Trks.	$\mu$ 's	Trks.	$\mu$ 's	Trks.
$\pi^+$ decay-in-flight	81 k	12 k	195 k	29 k	153 k	13 k
$\pi^-$ decay-in-flight	35 k	8 k	84 k	20 k	76 k	20 k
$K^+$ decay-in-flight	63 k	13 k	151 k	31 k	139 k	20 k
$K^-$ decay-in-flight	6 k	3 k	15 k	6 k	18 k	8 k
Total $\mu^+$	144 k	25 k	346 k	60 k	292 k	33 k
Total $\mu^-$	41 k	11 k	99 k	26 k	94 k	28 k

Expected single muon rates per  $2 \times 10^{12}$  protons from decay-in-flight mesons which pass through the detector ( $\mu$ 's) and satisfy trigger matrix tracking requirements (Trks.) from liquid hydrogen and deuterium targets and the copper beam dump.

## Conclusions

- Hodoscope concerns have been greatly decreased with finds of PMTs and scintillator from old experiments by P.R. and N.M..
- Station 1 will be the most worrisome plane, primarily due to rates and occupancy level. If the paddles are too wide, they likely will be “on” for every proton bucket.
- Single time bucket resolution appears to be simple for all cases.
- Some attention needs to be paid to effects on increasing the number of hodoscope paddles from 2x16 per plane to 2x32 per plane at Station 1 and possibly Station 2.
- Do we overlap hodoscope paddles? If so, by how much. Tradeoff is between rate limits and trigger capabilities.
- Having double-ended readouts for Stations 3 and 4 should not now be a problem since we won't need any of the old PMTs for Stations 1 and 2.



■ Extra Slides. Ignore.

### 3.4 Scintillator Hodoscopes

Scintillator hodoscope planes will provide the hit information for the hardware trigger system, just as they have in E866. There will be a total of eight planes, four to measure track  $y$  (bend plane) locations and four to measure track  $x$  locations. There will be a  $y$  hodoscope plane associated with each of the four detector stations – referred to as Y1, Y2, Y3, and Y4. They will contain 32 channels apiece, separated into 16 channels on the right side of the spectrometer ( $x < 0$ ) and 16 channels on the left side ( $x > 0$ ). There will be  $x$  hodoscope planes associated with detector stations 1 and 2, plus two additional planes as part of station 4 – referred to as X1, X2, X4A, and X4B. They will contain 32 channels apiece, separated into 16 channels for the lower half of the spectrometer ( $y < 0$ ) and 16 channels for the upper half ( $y > 0$ ). This segmentation will provide a logical division of each hodoscope plane into quadrants, allowing the trigger system to place tighter geometric constraints on the tracks than was done during E866.

All of the scintillators within a given  $y$  hodoscope plane will be the same size. The individual scintillators within hodoscope planes X4A and X4B will all be the same angular size. In contrast, the four X1 and four X2 scintillators closest to  $x = 0$  will subtend half the angular range, and the scintillators furthest from  $x = 0$  will subtend 1.5 times the angular range of the X4A and X4B scintillators and the remaining X1 and X2 scintillators. This segmentation minimizes the number of hodoscope channels in stations 1 and 2 that may be in coincidence with given channels in X4A and X4B, after accounting for the multiple scattering of the muons through the various absorbers in the spectrometer.

While many of the hodoscopes could be fabricated primarily by recutting and polishing the existing E866 scintillators to the sizes required for the new spectrometer, we believe it is safer, given their age, to plan on constructing new scintillators and light guides for this experiment. We propose to reuse the phototubes and bases from the existing E866 spectrometer and purchase 60 new phototubes and bases for the additional channels. The existing E866 high voltage distribution systems will suffice to power the eight hodoscope planes.

During E866, the anode signals from each phototube were sent to LeCroy 4416 leading-edge discriminators. The discriminator outputs were reshaped by custom synchronizer/stretcher modules to provide clean, single RF bucket time resolution for all hodoscope planes except station 4, which had slightly worse than single bucket resolution. The higher background rates anticipated at the Main Injector due to the increased beam current make it very important to achieve clean, single RF bucket time resolution for all hodoscope planes. Given past experience, this should be straightforward with the existing discriminators for the hodoscopes in stations 1 and 2, and for the X4A and X4B planes. The longest scintillators in the spectrometer, those for Y4, will be only 7" shorter than the station 4 scintillators during E866 and we propose to use phototubes on each end of these scintillators and 32 channels of mean timers to provide single bucket resolution. We already have enough synchronizer/stretcher modules in hand to instrument the entire new spectrometer.

### 3.6 Trigger

The hardware trigger system will examine the scintillator hodoscope hits to identify patterns characteristic of high mass muon pairs produced in the target. It will be conceptually similar to the system that was developed for E866 [27]. However, it will be enhanced substantially compared to the previous system, primarily to improve its ability to reject random coincidences that appear to form a candidate high  $p_t$  muon track. Such random coincidences represented over half of the apparent muon tracks observed during the E866 intermediate mass  $\bar{d}/\bar{u}$  running, and the background rates in the spectrometer due to soft muons are expected to be even higher at the Main Injector. The trigger modifications will also permit us to implement two-dimensional masking of wire chamber hits during event analysis, based on the active hodoscope roads, which will reduce the combinatorics in the wire chamber track finding. Notably, this will minimize the frequency of hit- and track-bank overflows, one of the sources of rate-dependent reconstruction inefficiency that we encountered during E866. Finally, the trigger modifications will permit us to replace a number of custom CAMAC modules from the E866 trigger system that are now nearly 20 years old with new, more reliable and flexible, commercial units.

Electronically, the hardware trigger will consist of a single decision stage, implemented as a three-step parallel pipeline. In the first step, the outputs from the hodoscope synchronizer/stretcher modules will be routed to a set of LeCroy 2367 Logic Modules. Eight modules will be dedicated to identifying four-fold Y1-Y2-Y3-Y4 coincidences characteristic of high  $p_t$  single muons produced in the target. Each time they observe a candidate track, they will output a bit indicating its charge, the side of the spectrometer (left or right) where it is located, the quadrant the track passed through at Y1, and the actual  $y$  location of the track at Y4. In general, Y1-Y2-Y4 triple coincidences would suffice since the spectrometer analyzing magnet is located between stations 1 and 2, and that is in fact how candidate tracks were identified during E866. Adding the extra constraint that the appropriate channel of Y3 must have a hit will help reject apparent tracks that actually consist of a random coincidence between hits in stations 1 and 2 due to one muon and a hit in station 4 due to another.



The  $\bar{d}/\bar{u}$  experiment will only be interested in a limited number of potential track roads through the spectrometer. However, the eight LeCroy 2367 modules required to identify all of those tracks contain enough additional internal logic and I/O capability to cover the entire phase space of four-fold Y1-Y2-Y3-Y4 coincidences associated with real tracks originating from either the target or the beam dump. This will provide maximal flexibility when designing triggers for study purposes or ancillary measurements.

Four additional LeCroy 2367 modules will be dedicated to identifying candidate tracks originating from the target that include coincidences among at least three of the four planes X1-X2-X4A-X4B. Each time they observe a candidate track, they will output a bit indicating the side of the spectrometer where it is located, the quadrant the track passed through at X1 and X2, and the actual  $x$  location of the track at X4A and X4B. This represents a significant upgrading of the tracking capability of the hardware trigger in the  $x$  direction, compared to E866, and will permit us to provide full two-dimensional constraints on the tracks. It will also make continuous monitoring of the efficiency of the  $y$  hodoscopes practical. This may prove to be important because our ability to average over long-term variations in the spectrometer efficiency between targets will be reduced at the Main Injector, since we will be unable to change amongst the various targets as frequently as we did during E866. In contrast, for E866 special hodoscope efficiency studies were run every few weeks. They consisted of a series of runs utilizing a special trigger configuration, sequentially turning off the high voltage on sets of  $x$  hodoscopes near the center of the spectrometer.



The second step in the trigger pipeline will combine the  $x$  and  $y$  tracking results from the first step to identify events with candidate high  $p_t$  muons present. This will be done in a pair of LeCroy 2367 modules, one dedicated to tracks on the left side of the spectrometer and one dedicated to tracks on the right side. The candidate muons will be characterized according to their charge, the side of the spectrometer on which they are located, and a rough measure of their  $p_t$ . Events will also be tagged that appear to have two muons with opposite charges present on the same side of the spectrometer.

In parallel with the first two steps of the main trigger sequence, OR's of all the scintillators on each side of each plane will be generated and routed to a Track Correlator [27] to generate simple cosmic ray and noise triggers for diagnostic purposes. This same procedure was utilized during E866, and the same CAMAC and NIM electronics will be reused at the Main Injector.

The final step in the trigger pipeline will generate the actual triggers, handle the experiment busy logic, and strobe the read-out electronics. This step will either be performed with one additional LeCroy 2367 module or with the Track Correlators and Master Trigger OR that were designed and constructed for the E866 hardware trigger [27]. The primary physics trigger will consist of a coincidence between two candidate  $x-y$  tracks of opposite charges, on either the same or opposite sides of the spectrometer. If we find that the background trigger rate due to low mass muon pairs is higher than desirable, we will combine the rough measures of the  $p_t$  for the two muons from the previous step to provide a crude effective mass cut on the muon pair in hardware. A similar procedure, but with less granularity than we anticipate with the new trigger system, was adopted for several of the data sets taken during E866. For example, it reduced the raw trigger rate during the E866 intermediate mass  $d/\bar{u}$  data taking by a factor of three, with essentially no reduction in efficiency for the Drell-Yan muon pairs of interest. Two triggers will be used to determine the rate of random coincidences between two muon tracks in the same RF bucket, both of which originate from the target and, thus, are indistinguishable from a real Drell-Yan muon pair. One of these triggers will record events that contain two muons of the same charge when they are located on opposite sides of the spectrometer, while the other will record a prescaled set of single-muon events. E866 has demonstrated that we can obtain an excellent simulation of the random coincidence background by combining muons from single-muon triggers into pairs, then normalizing their number to the observed rate of like-sign coincidences. Two additional triggers will select prescaled samples of events that contain a candidate track in either the  $x$  or  $y$  direction, but not necessarily both. The events with  $x$  tracks will be used to monitor the absolute efficiencies of the  $y$  hodoscopes, and the events with  $y$  tracks will be used to monitor the absolute efficiencies of the  $x$  hodoscopes. The last trigger will provide a luminosity-weighted read-out of all detector elements during random RF buckets, independent of the status of any of the spectrometer hodoscopes. This will be used to provide an unbiased measure of the background occupancy rates throughout the spectrometer, which are very important for estimating rate-dependent reconstruction inefficiencies.

Table 2: Wire Chamber Specifications and Singles Rates

Station	Type	x size (cm)	y size (cm)	wire spacing (mm)	wire orientations	Number of Channels	Singles Rates (MHz)
1	MWPC	94	137.2	2.0	Y, Y', U, U', V, V'	5500	40
2	DC	137.7	149.9	10.2	Y, Y', U, U', V, V'	1000	10
3	DC	203.0	162.4	20.3	Y, Y', U, U', V, V'	700	2
4	Prop. Tubes	250.0	250.0	50.8	Y, Y', X, X'	400	4

Table 4: Expected single muon rates per 1 s spill of  $10^{12}$  protons from decay-in-flight mesons which pass through the detector ( $\mu$ 's) and satisfy trigger matrix tracking requirements (Trks.) from liquid hydrogen and deuterium targets and the copper beam dump.

	$LH_2$ Target		$LD_2$ Target		Copper Beam Dump	
	$\mu$ 's	Trks.	$\mu$ 's	Trks.	$\mu$ 's	Trks.
$\pi^+$ decay-in-flight	40.6 k	6.1 k	97.7 k	14.6 k	75.9 k	6.5 k
$\pi^-$ decay-in-flight	17.4 k	4.1 k	41.9 k	9.8 k	38.2 k	10.1 k
$K^+$ decay-in-flight	31.5 k	6.5 k	75.8 k	15.6 k	69.6 k	10.3 k
$K^-$ decay-in-flight	3.1 k	1.3 k	7.6 k	3.1 k	8.8 k	4.2 k
Total $\mu^+$	72.1 k	12.6 k	173.5 k	30.2 k	145.5 k	16.8 k
Total $\mu^-$	20.5 k	5.4 k	49.5 k	12.9 k	47.0 k	14.3 k

### 3.4 Scintillator Hodoscopes

Scintillator hodoscope planes will provide the hit information for the hardware trigger system, just as they have in E866. Each of the four tracking station will have a  $y$ -measuring hodoscope plane associated with it. Each plane will have a total of 32 channels, separated into two groups of 16 channels for the left ( $x > 0$ ) and right ( $x < 0$ ) sides of the detector. There will be  $x$  hodoscope planes associated with detector Stations 1 and 2, plus two additional planes as part of Station 4. They will contain 32 channels apiece, separated into 16 channels for the lower half of the spectrometer ( $y < 0$ ) and 16 channels for the upper half ( $y > 0$ ). This segmentation will provide a logical division of each hodoscope plane into quadrants, allowing the trigger system to place tighter geometric constraints on the tracks than was done during E866.

All of the scintillators within a given  $y$  hodoscope plane will be the same size. The individual scintillators within hodoscope planes X4A and X4B will all be the same angular size. In contrast, the four X1 and four X2 scintillators closest to  $x = 0$  will subtend half the angular range, and the scintillators furthest from  $x = 0$  will subtend 1.5 times the angular range of the X4A and X4B scintillators and the remaining X1 and X2 scintillators. This segmentation minimizes the number of hodoscope channels in Stations 1 and 2 that may be in coincidence with given channels in X4A and X4B, after accounting for the multiple scattering of the muons through the various absorbers in the spectrometer.



For E866, the anode signals from each phototube were sent to LeCroy 4416 leading-edge discriminators. The discriminator outputs were reshaped by custom synchronizer/stretcher modules to provide clean, single RF bucket time resolution for all hodoscope planes except Station 4, which had slightly worse than single bucket resolution. The higher background rates anticipated at the Main Injector due to the increased beam current make it very important to achieve clean, single RF bucket time resolution for all hodoscope planes. Given past experience, this should be straightforward with the existing discriminators for the hodoscopes in Stations 1 and 2, and for the X4A and X4B planes. The longest scintillators in the spectrometer, those for Y4, will be only 7" shorter than the Station 4 scintillators during E866 and phototubes will be placed on each end of these scintillators. With the double-ended readout and mean timers single bucket resolution will be achieved. Enough synchronizer/stretcher modules are available to instrument the entire new spectrometer.



and constructed for the E866 hardware trigger [75]. The primary physics trigger will consist of a coincidence between two candidate  $x - y$  tracks of opposite charges, on either the same or opposite sides of the spectrometer. If the background trigger rate due to low mass muon pairs is higher than desirable, a rough measurement of the  $p_T$  for the two muons from the previous step may be added to provide a crude effective mass cut on the muon pair in hardware. A similar procedure, but with less granularity than anticipated with the new trigger system, was adopted for several of the data sets taken during E866. It reduced the raw trigger rate during the E866 intermediate mass  $\bar{d}/\bar{u}$  data taking by a factor of three, with essentially no reduction in efficiency for the Drell-Yan muon pairs of interest. Two triggers will be used to determine the rate of random coincidences between two muon tracks in the same RF bucket, both of which originate from the target and, thus, are

general, Y1-Y2-Y4 triple coincidences would suffice since the spectrometer analyzing magnet is located between Stations 1 and 2, and that is in fact how candidate tracks were identified during E866. Adding the extra constraint that the appropriate channel of Y3 must have a hit will help reject apparent tracks that actually consist of a random coincidence between hits in Stations 1 and 2 due to one muon and a hit in Station 4 due to another.

The  $\bar{d}/\bar{u}$  measurement will only be interested in a limited number of potential track roads through the spectrometer. However, the eight LeCroy 2367 modules required to identify all of those tracks contain enough additional internal logic and I/O capability to cover the entire phase space of four-fold Y1-Y2-Y3-Y4 coincidences associated with real tracks originating from either the target or the beam dump. This will provide maximal flexibility when designing triggers for study purposes or ancillary measurements.

Four additional LeCroy 2367 modules will be dedicated to identifying candidate tracks originating from the target that include coincidences among at least three of the four planes X1-X2-X4A-X4B. Each time they observe a candidate track, they will output a bit indicating the side of the spectrometer where it is located, the quadrant the track passed through at X1 and X2, and the actual  $x$  location of the track at X4A and X4B. This represents a significant upgrading of the tracking capability of the hardware trigger in the  $x$  direction, compared with E866, and will permit full two-dimensional constraints on the tracks. It will also make continuous monitoring of the efficiency of the  $y$  hodoscopes practical. This will be important because the ability to average over long-term variations in the spectrometer efficiency between targets will be reduced at the Main Injector, since it will be difficult to change amongst the various targets as frequently as was done during E866. In contrast, for E866 special hodoscope efficiency studies were run every few weeks. They consisted of a series of runs utilizing a special trigger configuration, sequentially turning off the high voltage on sets of  $x$  hodoscopes near the center of the spectrometer.

The second step in the trigger pipeline will combine the  $x$  and  $y$  tracking results from the first step to identify events with candidate high  $p_T$  muons present. This will be done in a pair of LeCroy 2367 modules, one dedicated to tracks on the left side of the spectrometer and one dedicated to tracks on the right side. The candidate muons will be characterized according to their charge, the side of the spectrometer on which they are located, and a rough measure of their  $p_T$ . Events will also be tagged that appear to have two muons with opposite charges present on the same side of the spectrometer.

In parallel with the first two steps of the main trigger sequence, OR's of all the scintillators on each side of each plane will be generated and routed to a Track Correlator [75] to generate simple cosmic ray and noise triggers for diagnostic purposes. This procedure was utilized during E866, and the same CAMAC and NIM electronics will be reused at the Main Injector.

The final step in the trigger pipeline will generate the actual triggers, handle the experiment busy logic, and strobe the read-out electronics. This step will either be performed with one additional LeCroy 2367 module or with the Track Correlators and Master Trigger OR that were designed and constructed for the E866 hardware trigger [75]. The primary physics trigger will consist of a coincidence between two candidate  $x - y$  tracks of opposite charges, on either the same or opposite sides of the spectrometer. If the background trigger rate due to low mass muon pairs is higher than desirable, a rough measurement of the  $p_T$  for the two muons from the previous step may be added to provide a crude effective mass cut on the muon pair in hardware. A similar procedure, but with less granularity than anticipated with the new trigger system, was adopted for several of the data sets taken during E866. It reduced the raw trigger rate during the E866 intermediate mass  $\bar{d}/\bar{u}$  data taking by a factor of three, with essentially no reduction in efficiency for the Drell-Yan muon pairs of interest. Two triggers will be used to determine the rate of random coincidences between two muon tracks in the same RF bucket, both of which originate from the target and, thus, are

Item	Responsible Group	Source
Station 1	Hodoscopes	
scintillator	ACU	New
phototubes	ACU	New
readout	ACU	New
Station 2	Hodoscopes	
scintillator	ACU	New
phototubes	ACU	New
readout	ACU	New
Station 3	Hodoscopes	
scintillator	ACU	New
phototubes	ACU	New
readout	ACU	New
Station 4	Hodoscopes	
scintillator	ACU	New
phototubes	ACU	New
readout	ACU	New



## Simple DAQ Systems for FPIX2 FPGA Development at LANL

PLM 12/11/06

We've assembled two DAQ systems to read out data from the FPIX2 through a Xilinx Virtex-4 FPGA development board. The goal was to use off the shelf components that require a minimum of programming to record the data. Optionally, the raw data is converted to a ROOT ntuple containing the hit row, column and amplitude value. We also have an Actel FPGA board that can be interfaced to these DAQ systems.

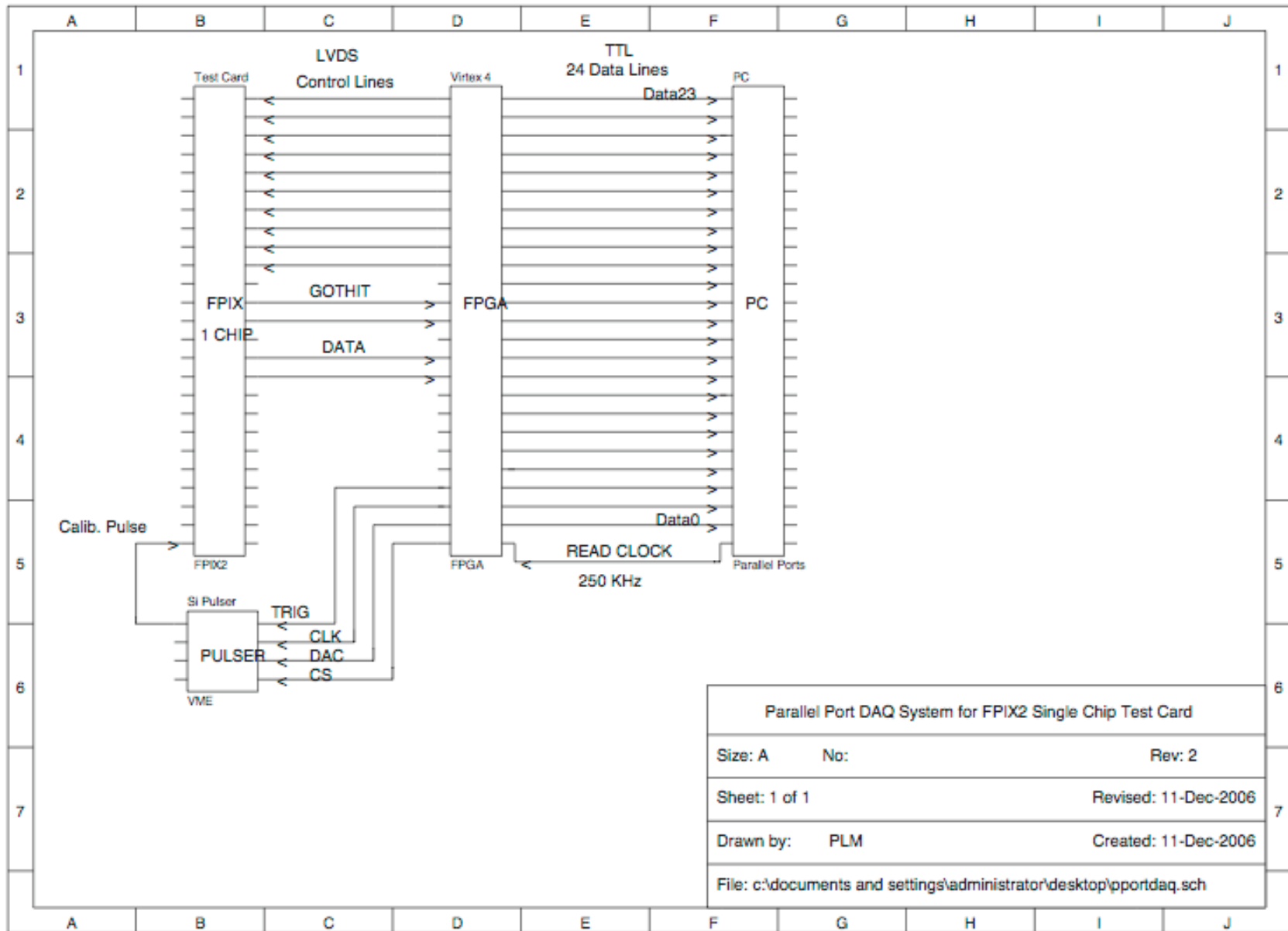


Figure 1. DAQ system for FPIX2 single chip test card using fast PC parallel ports

System 1. Provides ~1MB/sec sustained rate to disk/ntuple file. Three high-speed 8-bit parallel ports are used to read a 24-bit word from the FPGA, as shown in Figure 1. A control line from one port of the PC is used to clock the data from the output FIFO of the FPGA.

The parallel ports can operate in PS/2 mode or EPP mode (which is about twice as fast). The software is very simple linux C code using direct I/O through the parallel ports. This system is adequate for measuring the FPIX noise, channel by channel, in about ten minutes. The software can also be compiled to run under windows.

These PCI card based parallel ports are very inexpensive and easy to use. Data and clock lines are TTL, carried on regular ribbon cable. The FPGA output lines are set to 2.5 V CMOS. Interface connections between the FPGA, FPIX (single chip) and PC were bread-boarded using twisted pair and flat ribbon cabling.

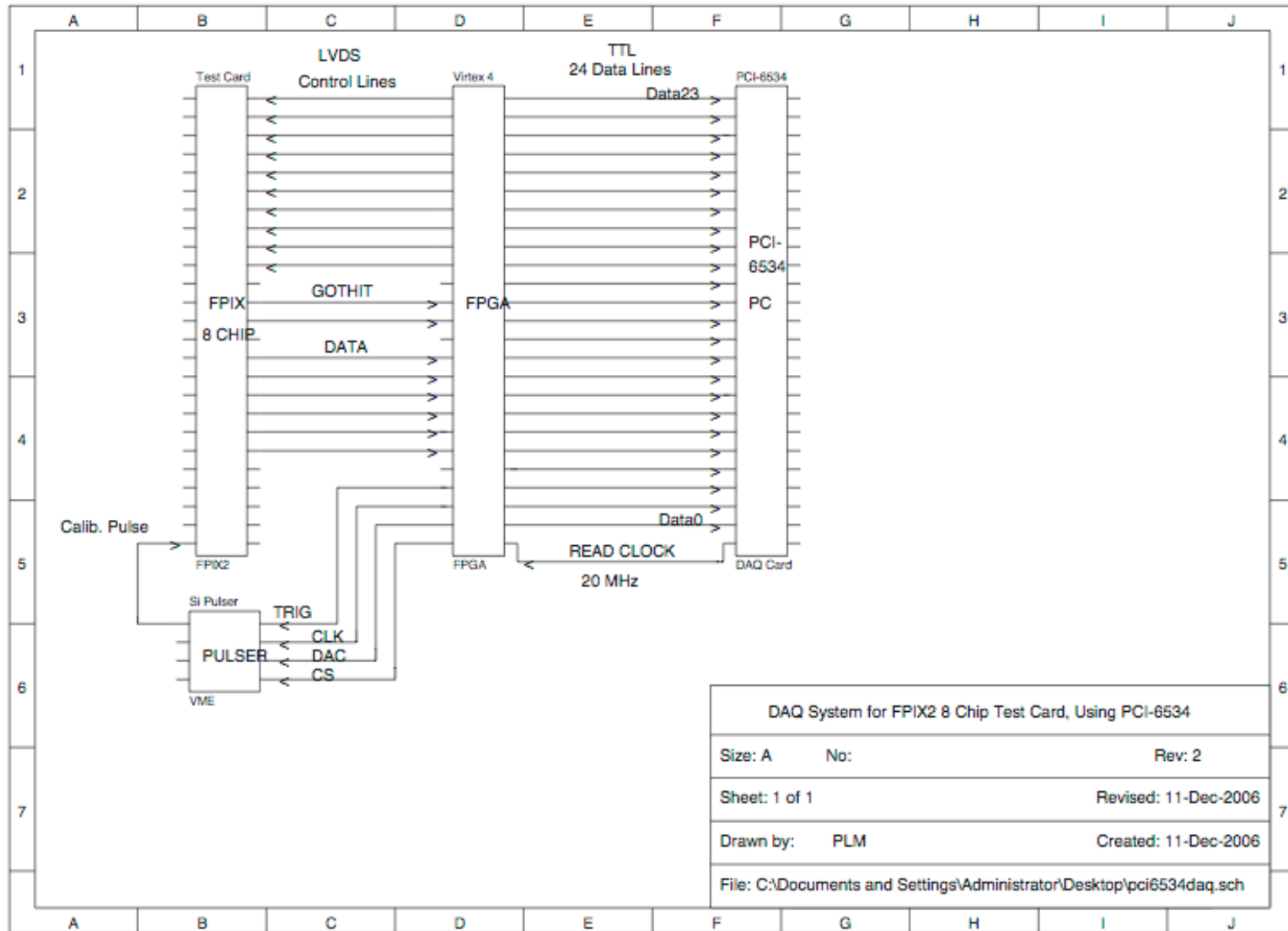


Figure 2. DAQ system for FPIX2 eight chip test card using NI PCI-6534 card.



System 2. Provides ~80MB/sec for a 64MB 32 bit transfer to memory. The sustained rate to disk has not yet been measured. This system uses the National Instrument PCI-6534 digital I/O card, as shown in Figure 2. Up to 32 bits of data can be collected at 20 MHz using pattern I/O. The PCI card generates pulses that are used as before to clock the data out of the FIFO. Cabling is done with commercial shielded twisted pair cable. The clock line is 5V TTL, resistively terminated and attenuated to 2.5V at the FPGA. The FPGA outputs are 2.5 V CMOS. The software is very simple, written in C for Windows using National Instrument's DAQmx driver.

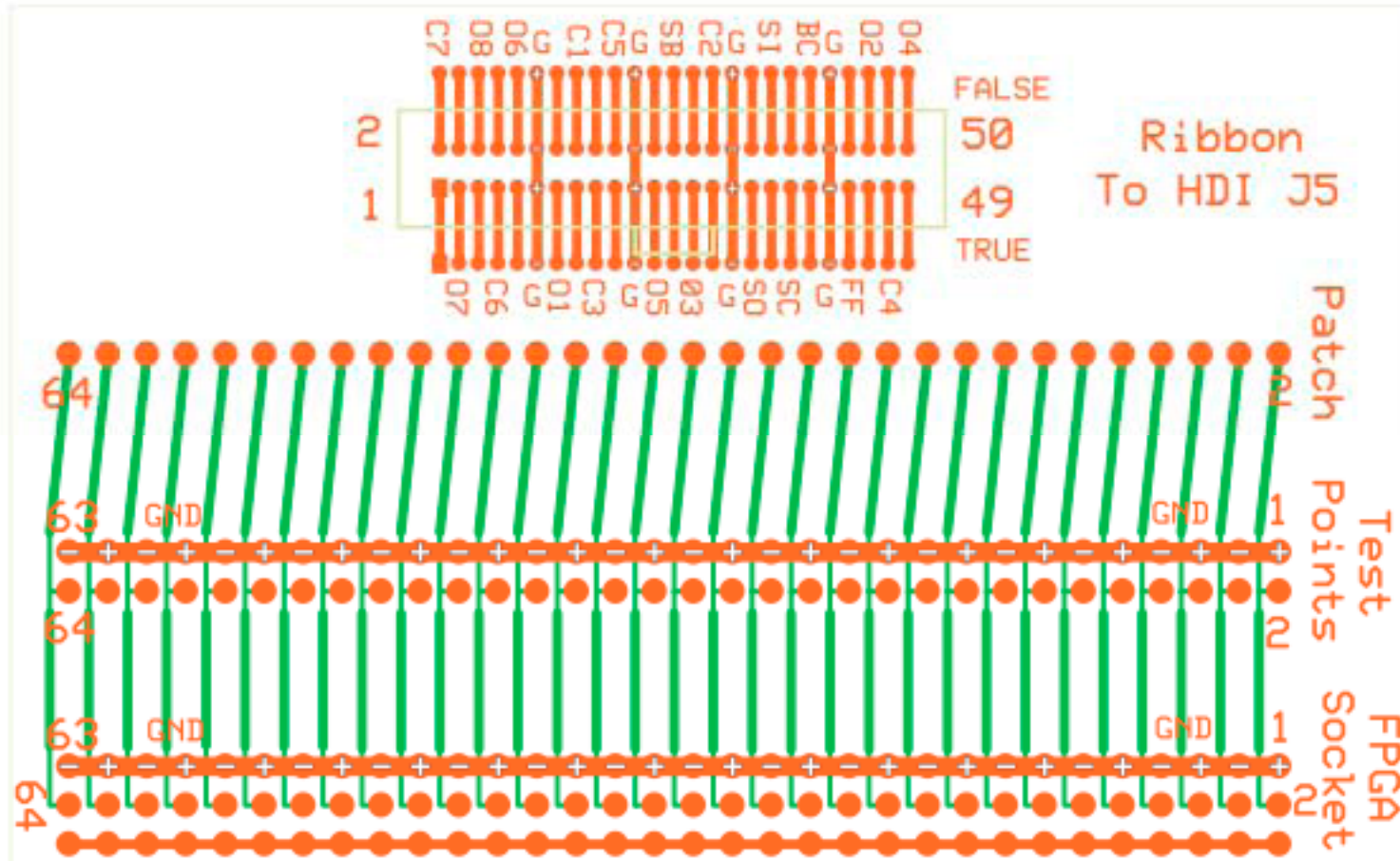


Figure 3. Interface card between FPIX 8 channel test card and Virtex 4 FPGA board. Top connector is attached through 50 pin .025 ribbon to FPIX. Bottom connector attaches to FPGA board.

We've used the PCI-6534 hardware to successfully read data at full speed from a 74F series TTL counter clocked at 20 MHz. We are presently connecting it to the FPGA board. This system appears capable of transferring data at the speed of existing PHENIX data collection modules. The PCI-6534 is somewhat expensive, costing about \$2000 for the card and shielded cable. Interfacing between the FPIX (on an 8 chip HDI test card) and the FPGA was done with a 4 layer PCB adapter card and twisted pair cabling (Figure 3). The FPGA to PCI card interface was done with a 2 layer PCB and shielded cable (Figure 4).

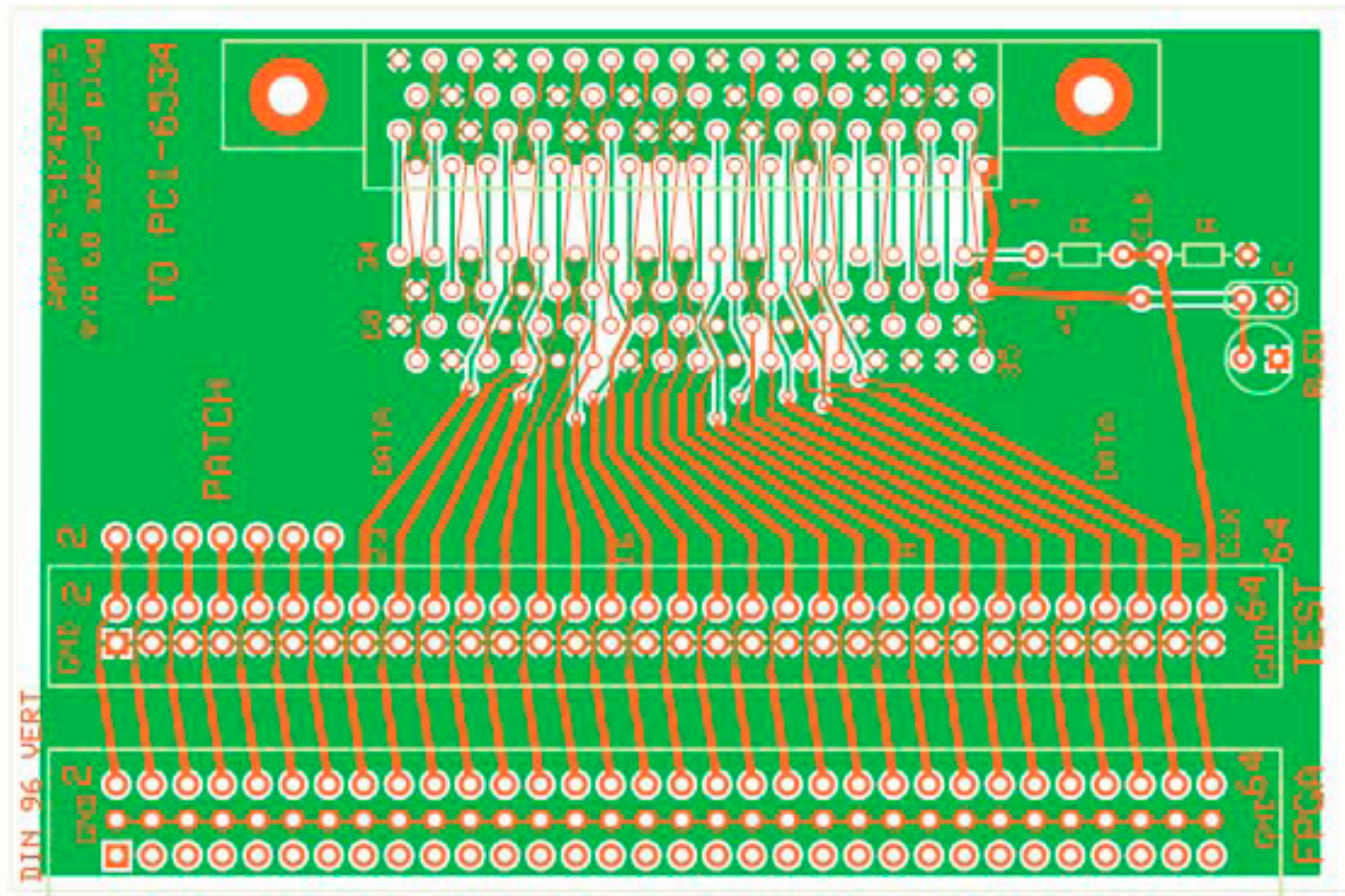


Figure 2. Interface card between Virtex 4 FPGA board and cable to PCI-6534. Top connector is for shielded cable to PCI-6534 card. Bottom connector attaches FPGA board.